

AUTOMATIC LAYERWISE ACQUISITION OF THERMAL AND GEOMETRIC DATA OF THE ELECTRON BEAM MELTING PROCESS USING INFRARED THERMOGRAPHY

Ridwan, S., Mireles, J., Gaytan, S.M., Espalin, D., Wicker, R.B.

W.M. Keck Center for 3D Innovation, The University of Texas at El Paso, El Paso, Texas

REVIEWED

Abstract

Layerwise monitoring has become an area of interest in the field of additive manufacturing because of potential to further enable part qualification during every stage of fabrication. Spatial monitoring and qualification during part fabrication has never before been possible with traditional manufacturing processes such as milling or casting. An IR camera has been externally annexed atop an EBM system to obtain layerwise thermographs throughout the fabrication process. This paper demonstrates a process to compare each layer of fabrication using automatically acquired thermal images to the corresponding CAD file for each fabricated object. Two different methods of image analysis for part detection were compared (analysis on the basis of color and analysis by edge detection). Detection allowed the quantification of processing information (average temperature and surface anomalies) and geometric information (surface area and perimeter). A percent error of the compared surface area was found to range from 5%-17%, and automatically acquired temperature measurements were within 7.8K of the recorded thermograph. The methods presented in this research showcase the beginning steps of integrated metrology in advanced manufacturing systems and automatic monitoring of per-part thermal behavior and part quality.

1.0 Introduction

Layerwise monitoring has become an area of interest in the field of additive manufacturing (AM) because of potential to further enable part qualification during every stage of fabrication. Previous thermal monitoring of layerwise processes like electron beam melting (EBM) has allowed characterization of defects that ultimately affect microstructure and part geometry [1, 2]. Dinwiddie *et al.* demonstrated a method of continuous thermal imaging within the Arcam EBM system that allowed post-fabrication evaluation of prevalent defects, such as porosity. Yadroitsev *et al.* demonstrated an optical system for molten pool temperature measurements using a charge-coupled device camera for the selective laser melting process where brightness temperature distributions were analyzed and microstructure changes were observed for biomedical components. Craig *et al.* developed a multi-sensor thermal imaging suite to monitor a directed energy deposition process. The authors also developed a software feature to measure variations of thermal metrics. Although the above mentioned works allowed for improved AM system feedback, there is still a need to implement automatic monitoring during fabrication.

In this research, a thermal camera has been installed atop an EBM system to monitor each layer after the melting process, or layer fabrication, has completed. A method for detecting the size, shape, and surface area of a fabricated object was accomplished. Additionally, an algorithm was developed to compare the thermal data obtained from the installed camera with an input layer derived from CAD as a means to detect any prevalent porosity. Furthermore, the pixel values from the obtained thermographs were converted to temperature values and averaged to obtain and record an average temperature value within the object's surface area. Such methods

of automatic temperature acquisition and layer-by-layer CAD to thermograph comparison showcase the beginning steps of integrated metrology in advanced manufacturing systems and automatic monitoring of per-part thermal behavior and part quality.

2.0 Methodology

AM processes typically begin through a stereolithography (STL) file that is generated from a CAD model that works on the basis of triangulation of the three-dimensional geometry. STL files can be of two types: binary and ASCII. Precision of the geometry is affected by the layer thickness of the successive layers, or slices, typically ranged between 0.05-0.2mm [3]. The STL file is then converted to the format supported by the machine, or a slice file (two-dimensional file) of the STL geometry, that contains the beam path instructions. Although part geometry is currently used as input via a CAD model, various nebulous factors such as differences with the ideal surface area, shape, and the fabrication conditions of the manufacturing process (i.e. prevalence of defects such as warping) affect a part's surface area.

In this research, a FLIR SC645 infrared (IR) camera (FLIR Systems, Wilsonville, OR) was used to automatically output thermal images from each layer of a part's surface area. The camera was tilted to 15 degrees with respect to the vertical axis of the fabrication chamber and views fabrication through a ZnSe glass. The installation of the IR camera in EBM is described in more detail in previous research work [3, 4]. A pneumatic system controls a shutter mechanism that protects the camera's viewing window from metallization, or a coating phenomenon that occurs during melting [4]. A control system using LabVIEW (National Instruments, Austin, TX) was developed to control the shutter mechanism and automatically acquire thermal images of each layer after the melting process was completed [3, 4]. Voltage signals from the EBM system were acquired during the build process and interpreted by a modular controller (NI cRIO-9074, National Instruments, Austin, TX). These signals were used to automatically acquire thermographs from the build area. Using LabVIEW, thermographs were saved as bitmap images where each pixel value represented a temperature value after the melting process of the built object for each specific layer. Using the image and data acquired from the camera, a MATLAB (The MathWorks, Inc., Natick, MA) code was developed to obtain the desired image data, detect defects of an object, and find the average temperature value during/after the melting process.

Using MATLAB, a region of interest was selected on the basis of the graphical input where four coordinates were selected manually at the beginning of image analysis. A matrix was formed on the basis of minimum and maximum values of X and Y coordinates to ensure that all fabricated objects were within the region of interest. The original image was then converted into a binary image, and boundaries were detected to identify the fabricated parts using two different techniques (edge detection and detection on the basis of color difference). The pixel values within the boundaries were read from the standardized image and converted to temperature values, and average temperature values were calculated for each fabricated part. Furthermore, the surface area (total number of pixels) and perimeter were obtained for each detected part. Finally, the ideal surface area for the fabricated object was measured from input layerwise data and a percent error from each surface area measured was calculated.

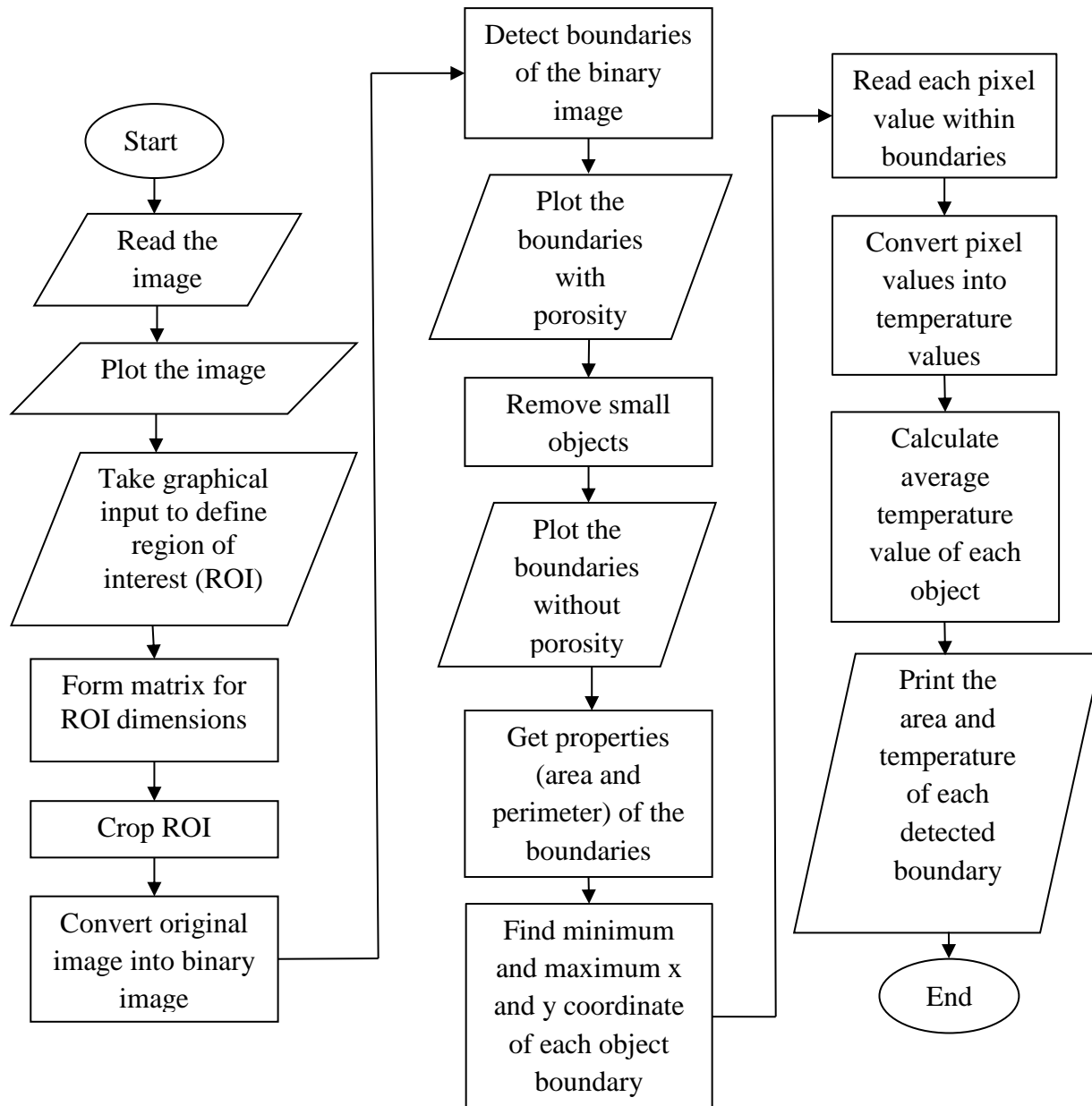


Figure 1. Flowchart of steps for analysis of output layer based on color.

2.1 Algorithms

Two different techniques were followed to analyze the output thermographs after the melting process: 1) analysis on the basis of color and 2) analysis on the basis of an edge detection technique. The steps in the analysis of the output layer on the basis of color are depicted in Figure 1.

Analysis on the basis of color begins by taking the original image, cropping to segment fabrication area, and the detecting and labeling of boundaries for analysis. Pixels within the detected boundaries allowed the calculation of geometric variables such as surface area and perimeter as well as process variables such as average temperature values. For geometry, the

area of each pixel was previously calibrated [4] and used in this study for calculation. To calculate part temperature, pixel brightness was converted to a temperature value using the previously developed conversion method [3]. Upon calculation of necessary parameters, the code prints all the acquired data on-the-fly. Basic steps in edge detection technique utilized for this study are shown by Figure 2.

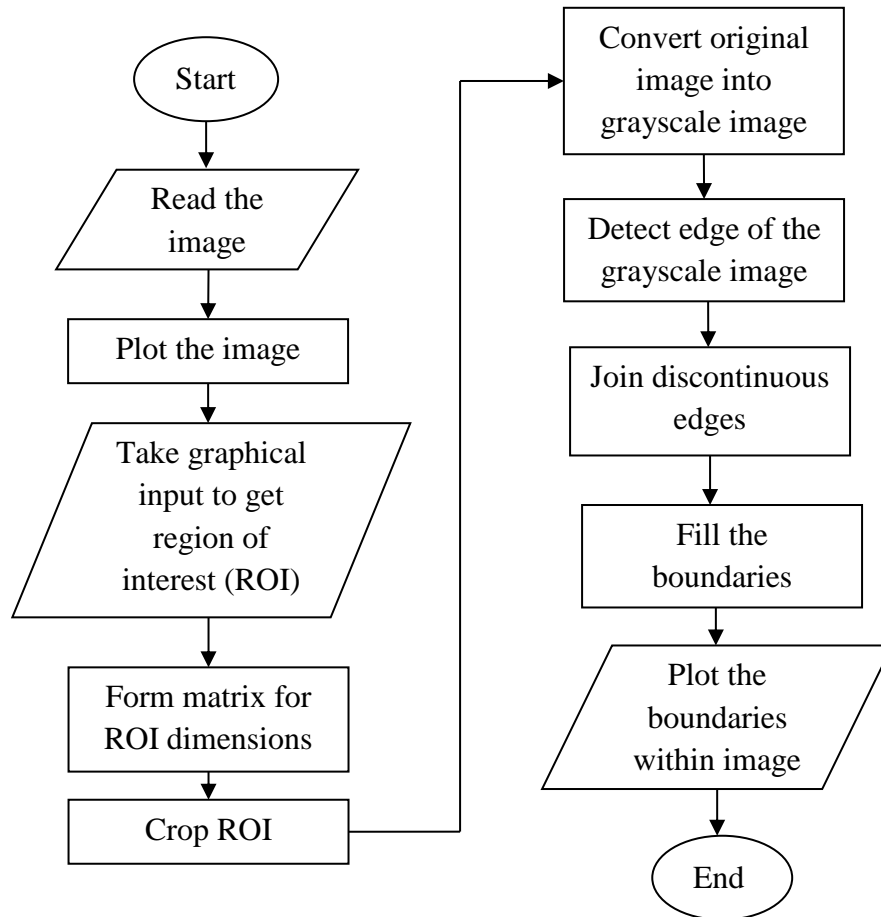


Figure 2. Flowchart of steps for analysis of output layer based on edge detection technique.

The Sobel method, which is an image analysis method based on image intensity values, was used for edge detection. In this method, instead of detecting boundaries from the cropped color image obtained, the cropped image was converted to grayscale to facilitate edge detection. Discontinuous edges were joined, and boundaries were filled to get an image of the fabricated object. Geometric and process variables were also capable of being obtained upon acquiring the image of the fabricated object.

Although both of the above steps allow geometric measurement of fabricated parts, comparison of the ideal geometry is necessary for part qualification applications. In this study, measured geometry was compared to the ideal slice data from the input CAD file. A MATLAB code was developed to compare the input layer (ideal slice image) with the output layer (thermal image). The steps for comparison are depicted in Figure 3.

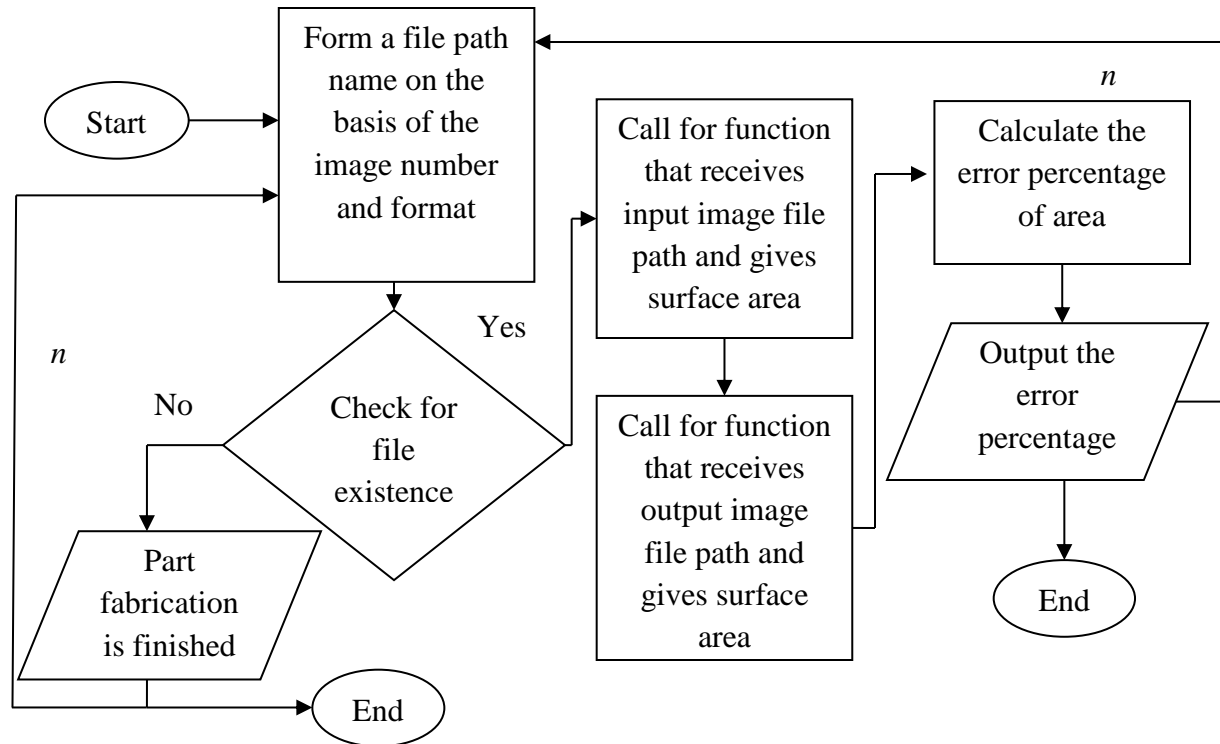


Figure 3. Flowchart of steps for comparison of input and output layer.

Comparison of the detected surface area starts by first matching the file name (corresponding to the layer being compared) corresponding to the current layer. If the file name for the ideal image matches that of the image being compared, comparison of surface area continues until fabrication is complete. Here, two different script files were called to obtain the surface area for input and output layers. The first function script used the color difference technique (as described in Figure 1) and returned the surface area. In Figure 3, n is the number of iterations that depends on the number of layers of the built object as well as the number of images of the output layer after the object's melting process has completed. Before the calculation of the error percentage, the size of the area matrix of both input and output layer images were also verified to ensure that the number of objects in both images were the same. A percent error was calculated upon comparison of both surface areas and recorded for each specific layer.

3.0 Results and discussion:

An example IR image (after cropping) is shown in Figure 4a. This represents the image used for detection on the basis of color (Figure 1). This original image is a representation of temperature, where lighter color represents higher temperature and darker color represents lower temperature (dependent on emissivity). Here, the build area of a particular layer, distinct (darker) low temperature regions from the thermal image can be seen within the solid cylinders being fabricated in this example. An example standardized grayscale image used for analysis on the basis of edge detection is shown in Figure 4b. The brightness differences shown by the

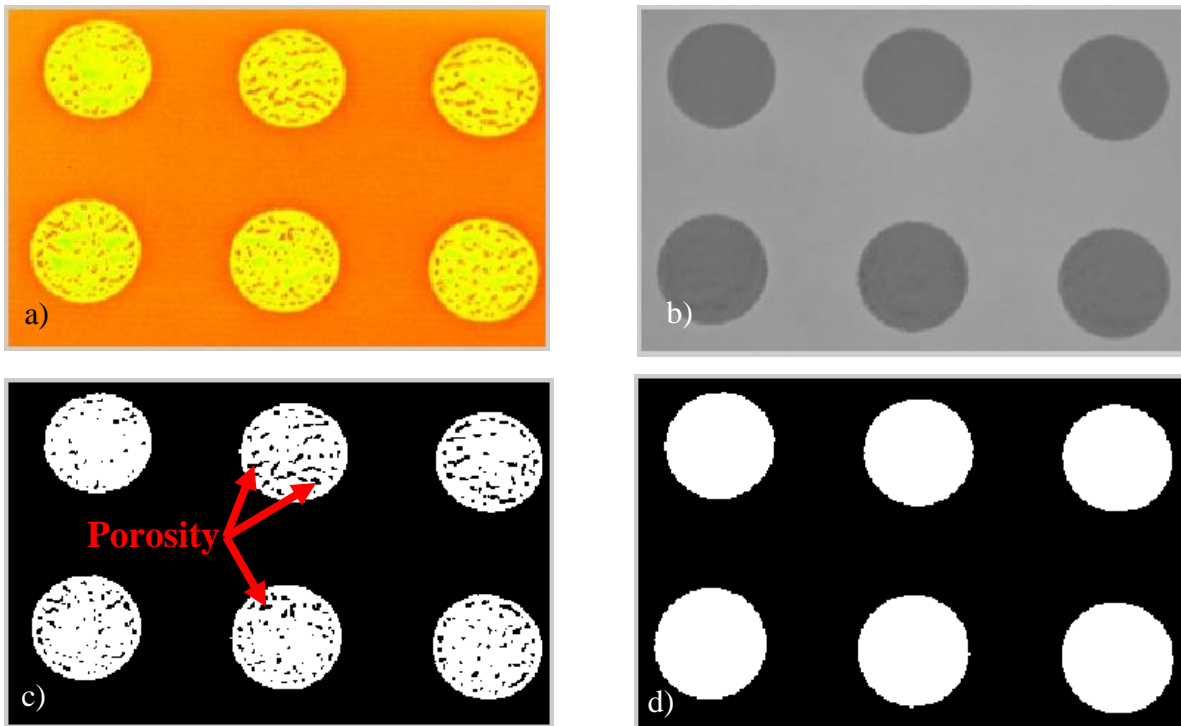


Figure 4. Original image (a), standardized grayscale image (b), binary image of original image (c) and inverted binary image of standardized grayscale image (d).

grayscale image (Figure 4b) represent temperature differences that, upon conversion, can be quantified as a temperature value. Figure 4c represents the binary image generated from the original thermal image, and Figure 4d represents the inverted binary image of the standardized grayscale image. If the melting is not appropriate, void spaces will occupy the melted region, which can cause porosity in fabricated parts. In the binary image (Figure 4c), distinct porous regions can be identified (shown by the black color) within the supposed melt area. Furthermore, Figure 4d represents a segmentation of the supposed melt area that is used for geometry measurements.

In Figure 5a, the boundaries were detected in the binary image, where the boundaries of the object can be observed in red (outer boundaries of fabricated cylinders). The red boundaries represent the object shape and area, and, porosity can be observed as child boundaries with green

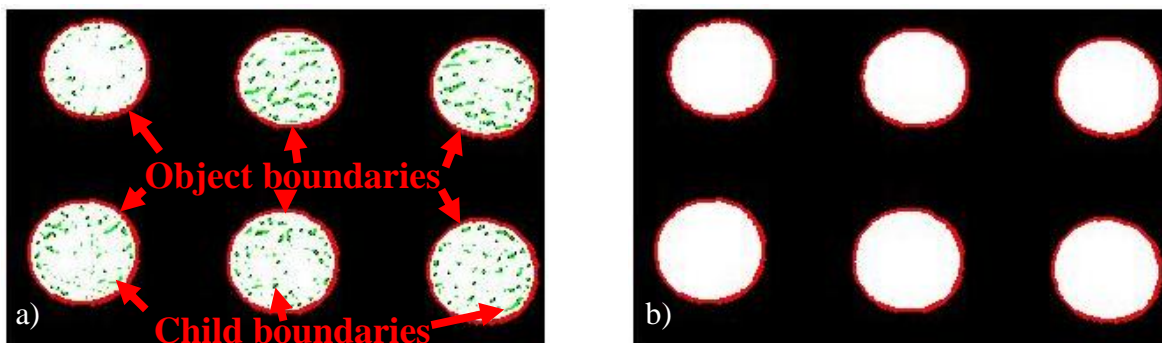


Figure 5. Porosity as child boundaries (a) and boundaries of objects (b)

boundaries (boundaries within melt region). The small areas (porosity) covering less than 300 pixels were identified and later removed to obtain the overall size of the supposed melt area (Figure 5b). In this case, the binary image was converted to an inverted binary image and the small areas (porosity) were removed. The inverted binary image was inverted again to remove any residual areas within the image. In Figure 5b white areas represent the fabricated objects, and black areas represent the non-melting zone (powder bed) of each layer.

No. of objects detected=6				
Object No.	Perimeter (pixel)	Area (pixel)	Temperature (K)	Type
1	203	3010	1483	Circular
2	197	2802	1481	Circular
3	205	3013	1505	Circular
4	197	2822	1502	Circular
5	196	2836	1490	Circular
6	203	3023	1501	Circular

Figure 6. MATLAB output.

Using a nested for loop and a conditional statement, the pixel values within each object boundary were read from the standardized image matrix, and all the pixel values were converted to temperature values. The average temperature values were calculated and printed as upshot in the MATLAB command window (Figure 6). Here, the area of detected object from the thermal image is based on a quantity of pixels detected where each pixel dimensionally represented a value of 170 microns [4]. A rounding error in the average temperature calculation (Figure 6) may be prevalent upon conversion. The maximum possible average temperature deviation was $\sim 7.8\text{K}$, depending on the round off error of each pixel value.

The second technique compared was the use of edge detection, where the original image was converted to a grayscale image and edge detection was performed. Figure 7a represents the image after the detection of the edge in the grayscale image. In some cases, a discontinuous edge can be observed after edge detection. The edges were joined where the pixel of a discontinuity was near another pixel within a radius of four pixels. A defect of area in the fifth and the sixth object in the image (Figure 7b) can be seen that occurred due to discontinuous edges. Furthermore, the boundaries of the output layer were not precisely circular after the melting process, as shown in Figure 8a, which represents a graphical plot of the boundary for a single

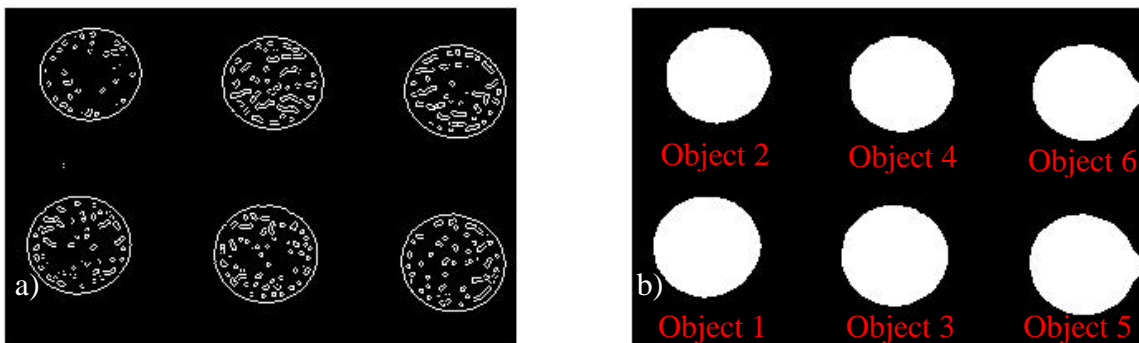


Figure 7. Edge detected in the image (a) and object after filling the edge area (b).

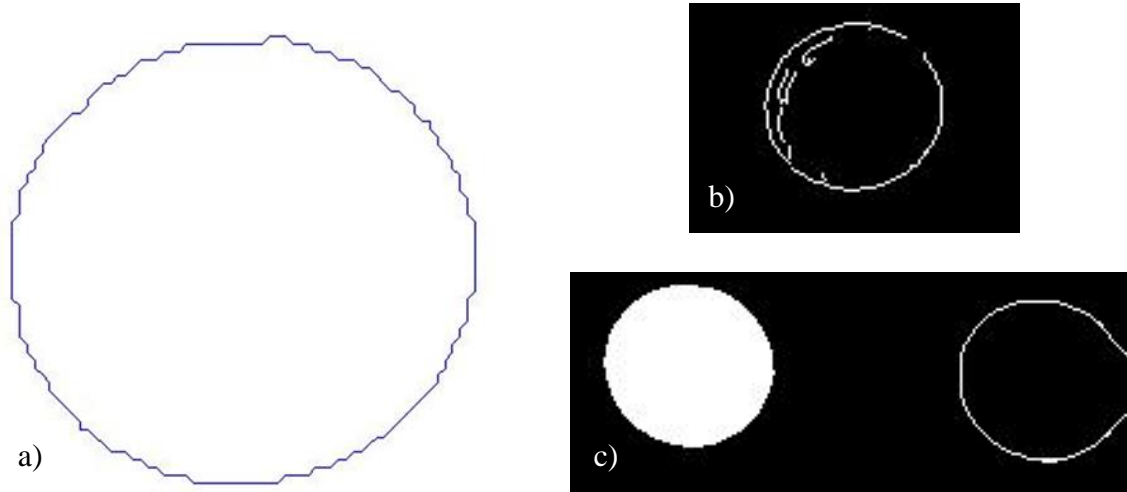


Figure 8. Showing detected boundary of an object (a) having jagged edges that affect measurement, discontinuous edges (b), and unfilled boundary for an object (c).

object. The jagged edges in Figure 8a can be explained by the system’s fabrication resolution or camera resolution. In some cases, the discontinuous edges cannot be joined if the pixels on the edge do not meet within the radius of 4 pixels (Figure 8b). As a result, the object is incorrectly detected for discontinuous boundaries (Figure 8c). Because of the erroneous surface areas found and its consequence on average temperature values, the temperature measurement technique was omitted using the edge detection algorithm. Hence, the edge detection technique was not sufficient to check the precision of the output layer or compare with an input layer.

Based on the algorithm mentioned earlier, the percentage error was found for each object of the selected layer after melting and compared to the ideal dimensions from CAD. Table 1 shows the data of error percentages for the area compared to the input layer of seven different thermal images corresponding to different fabrication layers. It was found that a different percent error of the fabricated area was found for each layer (always oversized from the CAD measurement). The range of percent error for object 5, for example, is 7.1% -16% and 5.4%-14% for object 6. The differences among fabricated areas between layers can be caused by corrugated surfaces of a built object, camera resolution, resolution of the fabrication system, and/or the material’s coefficient of thermal expansion (since images were taken during a heated environment).

Table 1. Error percentage of surface area pertaining to seven different images compared to their corresponding input layer images

	Object 1 error (%)	Object 2 error (%)	Object 3 error (%)	Object 4 error (%)	Object 5 error (%)	Object 6 error (%)
Layer 1	16	6.9	15	6.5	7.1	14
Layer 2	17	7.7	15	7.1	16	8.1
Layer 3	16	6.1	15	5.2	13	5.4
Layer 4	16	6.1	15	6.0	7.6	15
Layer 5	17	7.5	16	7.1	16	8.2
Layer 6	16	6.7	15	5.8	13	5.9
Layer 7	16	8.0	15	7.7	14	9.2

4.0 Conclusion

The methods presented in this research showcase the beginning steps of integrated metrology in advanced manufacturing systems and automatic monitoring of per-part thermal behavior and part quality. On the basis of analysis, thermal images provided sufficient data for the researchers to monitor and analyze the characteristics of EBM-fabricated objects. Two different methods for image analysis were compared, and it was determined that analysis on the basis of color was ideal for the images obtained in this research. Other methods of image analysis can be evaluated in future work. The geometrical data obtained in this study give a rough approximation as to the precision of the manufacturing process. Although a thermal camera was used in this study, higher resolution cameras can provide a better indication of fabrication precision on the basis of geometry. Furthermore, the geometric errors observed in this study can be attributed to various factors, including camera resolution, system resolutions, and the material's coefficient of thermal expansion (since images were taken during a heated environment). The MATLAB code generated in this study can be applied to other AM build processes, and further improvements of the software can be implemented that use the obtained data from the image for full spatial and temporal control as a means to obtain desired part mechanical properties. Furthermore, obtaining an indication of porosity was demonstrated in this study which can be used to perform parameter modifications that can help improve part quality and further lead to part qualification.

Acknowledgements

The research presented here was performed at The University of Texas at El Paso (UTEP) within the W.M. Keck Center for 3D Innovation (Keck Center), expanding recently to over 13,000 sq. ft. and providing access to state-of-the-art facilities and equipment as a result of funding, most recently, from the State of Texas Emerging Technology Fund. Support was provided, in part, by NIST grant 226351271A as well as the Mr. and Mrs. MacIntosh Murchison Chair I in Engineering Endowment. The authors are grateful for the assistance of Diego Mejorado and Heimdall Mendoza of the Keck Center on various aspects of the project.

References

1. Chlebus, E., Kuźnicka, B., Kurzynowski, T., & Dybała, B. (2011). Microstructure and mechanical behaviour of Ti—6Al—7Nb alloy produced by selective laser melting. *Materials Characterization*, 62(5), 488-495.
2. Parthasarathy, J., Starly, B., Raman, S., & Christensen, A. (2010). Mechanical evaluation of porous titanium (Ti6Al4V) structures with electron beam melting (EBM). *Journal of the mechanical behavior of biomedical materials*, 3(3), 249-259.
3. Rodriguez, E., (2013). Development of a thermal imaging feedback control system in electron beam melting. Master's thesis for master's degree, University of Texas at El Paso, El Paso, Texas, USA.
4. Mireles, J., (2013). Process study and control of electron beam melting technology using infrared thermography. Master's thesis for master's degree, University of Texas at El Paso, Texas, USA.
5. Dinwiddie, R. B., Dehoff, R. R., Lloyd, P. D., Lowe, L. E., & Ulrich, J. B. (2013, May). Thermographic in-situ process monitoring of the electron-beam melting technology used

- in additive manufacturing. In *SPIE Defense, Security, and Sensing* (pp. 87050K-87050K). International Society for Optics and Photonics.
6. Yadroitsev, I., Krakhmalev, P., & Yadroitsava, I. (2014). Selective laser melting of Ti6Al4V alloy for biomedical applications: Temperature monitoring and microstructural evolution. *Journal of Alloys and Compounds*, 583, 404-409.
 7. Craig, J. (2014, June). Multi-sensing Process Monitoring and Control of Directed Energy AM Processes. In *25th Advanced Aerospace Materials and Processes (AeroMat) Conference and Exposition (June 16-19, 2014)*. Asm.
 8. Deshpande, S., Kulkarni, A., Sampath, S., & Herman, H. (2004). Application of image analysis for characterization of porosity in thermal spray coatings and correlation with small angle neutron scattering. *Surface and coatings technology*, 187(1), 6-16.
 9. Pavlidis, I., & Levine, J. (2002). Thermal image analysis for polygraph testing. *Engineering in Medicine and Biology Magazine, IEEE*, 21(6), 56-64.
 10. Nandhakumar, N., & Aggarwal, J. K. (1988). Integrated analysis of thermal and visual images for scene interpretation. *Pattern Analysis and Machine Intelligence, IEEE Transactions on*, 10(4), 469-481.
 11. Nandhakumar, N., & Aggarwal, J. K. (1986, March). Integrating information from thermal and visual images for scene analysis. In *1986 Technical Symposium Southeast* (pp. 132-142). International Society for Optics and Photonics.
 12. Zhou, X., He, J., Liao, L. S., Lu, M., Ding, X. M., Hou, X. Y., ... & Lee, S. T. (2000). Real-time observation of temperature rise and thermal breakdown processes in organic LEDs using an IR imaging and analysis system. *Advanced Materials*, 12(4), 265-269.
 13. Kääb, A., & Vollmer, M. (2000). Surface geometry, thickness changes and flow fields on creeping mountain permafrost: automatic extraction by digital image analysis. *Permafrost and Periglacial Processes*, 11(4), 315-326.
 14. Murr, L. E., Gaytan, S. M., Medina, F., Martinez, E., Martinez, J. L., Hernandez, D. H., ... & Wicker, R. B. (2010). Characterization of Ti-6Al-4V open cellular foams fabricated by additive manufacturing using electron beam melting. *Materials Science and Engineering: A*, 527(7), 1861-1868.
 15. Murr, L. E., Esquivel, E. V., Quinones, S. A., Gaytan, S. M., Lopez, M. I., Martinez, E. Y., ... & Wicker, R. B. (2009). Microstructures and mechanical properties of electron beam-rapid manufactured Ti-6Al-4V biomedical prototypes compared to wrought Ti-6Al-4V. *Materials Characterization*, 60(2), 96-105.